MSc in Photonics

PHOTONICS**BCN**

Universitat Politècnica de Catalunya (UPC)
Universitat Autònoma de Barcelona (UAB)
Universitat de Barcelona (UB)
Institut de Ciències Fotòniques (ICFO)

http://www.photonicsbcn.eu

Master in Photonics

MASTER THESIS WORK

Radiometric simulation of LADAR imaging for underwater environments

Thomas Riley Morris II

Supervised by Dr. Santiago Royo, UPC and CD6

Presented on date 8th September 2014

Registered at

Escola Tècnica Superior d'Enginyeria de Telecomunicació de Barcelona

Radiometric simulation of LADAR imaging for underwater environments

Thomas R. Morris II

Centre for Sensors, Instruments and Systems (CD6)
UPC-BarcelonaTech, Rambla Sant Nebridi 10, Barcelona 08222, Spain

E-mail: photonics@trmorris.com

September 2014

Abstract. A Matlab framework to be used as an engineering tool for evaluating radiometric aspects of LADAR systems in underwater conditions is designed, validated, and demonstrated. The fundamental aspects of LADAR radiometry and imaging are discussed in addition to the supporting theories for the behavior of laser beam propagation in underwater environments with absorbing and scattering particles. Thorough testing is discussed that gives evidence to the validity of the model followed by application for an example design used in the Mediterranean Sea.

Keywords: LADAR, Remote, Sensing, Imaging, Ocean

1. Introduction

Laser detection and ranging (LADAR) is one of many types of remote sensing that has an increasing demand in a broad range of applications. LADAR is fundamentally similar to its predecessor, RADAR, with the main difference being that it is carried out with electromagnetic radiation at a much smaller wavelength and greater frequency. LADAR is a specific type of light detection and ranging (LiDAR) that uses a laser to produce light pulses; both technologies are based on time of flight (TOF) for the light pulses. The purpose of LADAR is similar to RADAR in that both technologies are able to make images with quantitative information about the distances of objects in the surrounding environment. However, due to the differences in wavelengths, each technology is used for specific

types of imaging. RADAR operates around the radio frequencies of 1MHz while LADAR operates near the visible portion of the spectrum on the order of 10^{14}Hz. The spatial resolution limits for both the surface morphology as well as the macro objects are dependent on the portion of the spectrum that is utilized. While RADAR is able to image very large objects with little surface detail, LADAR more effectively images detailed surfaces features. [1].

LADAR has been employed extensively for both atmospheric and oceanic purposes such as pollutant detection, landscape topography, and above-water mapping of the ocean. Next generation technologies like autonomous underwater vehicle automation will be dependent on real-time 3D mapping of the local environment [2] [3]. For these tasks, LADAR is a promising solution. However the amount of attenuation due to absorbing and scattering particles found in natural bodies of water can greatly reduce the received signal. Therefore, a rudimentary understanding of the radiometric limitations for different water conditions is required to enable these future technologies in fully submerged environments. It is the goal of this work to develop the first stages of a Matlab framework for radiometric modeling of LADAR systems in underwater conditions. The framework will prove to be useful as a future engineering tool for evaluating radiometric aspects during the design process [4].

LADAR relies on the time of flight of pulsed laser energy for determining range of objects in a given scene. TOF is the quantity of time from the moment the laser pulse leaves the emitter to the moment it returns to the detector by reflecting off of objects in the scene. Because the pulse must travel twice the distance of the range, the TOF divided by two is directly related to the range by the speed of light as follows, $R = (TOF/2)c$. This model will simulate a Gaussian shaped laser pulse as it is emitted, reflected, and detected with a focus on the radiometric distributions. In Section 2 the theoretical models that were applied to calculate the radiometric values at the detector will be presented along with a discussion of ambient oceanic effects on radiometry. Section 3 will present the steps that were taken to validate the Matlab model. Section 4 will discuss the simulation results for an oceanic environment.

2. Theoretical description

2.1. LADAR imaging

The two main types of LADAR systems are single point and imaging. The first type of system uses a single laser and photodetector such that the spatial information is limited to a single point in the propagation direction. The second type of system is able to image in 3D. This can be carried out by adding a scanning laser system to the single point LADAR system so that it will rasterize an image normal to the propagation direction. Another imaging method uses an array of photodetectors so that we obtain both temporal and spatial information with each pulse of laser energy. Though we are able to gain spatial information using an array of photodetectors, there is often a need for scanning the scene in order to obtain a detailed image [1]. Multiple sources and multiple detectors is also an option for imaging with LADAR. In the case of weak signals even single photon detection can be achieved using a Geiger-mode avalanche photodiode (GmAPD) [5] for either single point or imaging systems. Because this study is interested in developing the radiometric aspect of LADAR, the simulation will assume a single laser and a single array of photodetectors without scanning.

The first step in developing a radiometric model is to define each transformation during the flight of a pulse of light. These transformations include spatial and temporal distributions of energy in the laser pulse, the light intensity on the target surface, the reflected power from the surface, the reflected light intensity on the aperture, the power of light that passes through the aperture, the power that arrives to the detector, and finally the noise that is added to the signal at the detector. Each of these transformations have varying effects on the final power at the detector. The radiometric result of these transformations is given by equation 1, and it is known as the general solution to the range equation[1].

$$P_{det}\left(m,n,k\right)=\frac{\tau_o\tau_a^2 D_R^2\rho_t\left(dA\right)P_t\left(m,n,k\right)}{R^2\theta_R\left(\theta_t R\right)^2} \tag{1}$$

Where τ_o is the optical transmission, τ_a is the ambient transmission, D_R is the aperture diameter, ρ_t is the reflectivity, dA is the area of the distant array, P_t is the power of the laser pulse, R is the range, θ_R is the angle of radiative dispersion, and θ_t is the angular divergence. This form of the range equation denotes the discrete spatial samples of the field of view (FOV) by m and n while the discrete temporal samples are denoted by k. The the range gate determines the sampling time when the signal will be captured. It is specified by a minimum and maximum

TOF that corresponds to the range limits where the scene will be observed. This relationship is given as a modified version of the time of flight in equation 2 [1].

$$R_{gate} = (T_{\max} - T_{\min})\, c/2 \tag{2}$$

2.2. Beam propagation

The shape of the beam at the laser cavity can be spatially modeled as a Gaussian pulse given by equation 3. Where A_g is the complex amplitude of the beam's electric field, ω_o is the beam width of the pulse at $z = 0$ also known as the beam waist [1].

$$g_{LC}\left(x_m, y_n\right) = A_g e^{\frac{-\left(x_m^2 + y_n^2\right)}{\omega_0^2}} \tag{3}$$

A spatial Gaussian distribution assumes that the laser beam is propagating in the fundamental transverse mode, TEM00. Free space propagation of the beam results in divergence of the beam width according to equation 4. Where z is the propagation distance and λ is the wavelength. This is true for distances that are less than the Rayleigh length [6].

$$\omega\left(z\right) = \omega_0 \sqrt{1 + \left(\frac{z\lambda}{\pi\omega_0^2}\right)^2} \tag{4}$$

The laser pulse is also modeled as a Gaussian function in time. Equation 5 shows the power distribution where σ_w is the temporal width of the pulse and E_t is the energy of the pulse [6].

$$P_t\left(t\right) = \frac{E_t}{\sigma_w \sqrt{2\pi}} e^{\frac{-t^2}{2\sigma_w^2}} \tag{5}$$

2.3. Ambient effects

In most cases the extent of the range and the ambient transmission are the greatest causes of signal reduction. The reduction of transmitted light is primarily due to the attenuation caused by absorption and scattering of the particles that are suspended in the medium. Because the transmission is a function of range, the ambient conditions become one of the most important aspects that will determine the signal-to-noise ratio (SNR) and the amount of gain that is required to interpret the signal. Absorption is considered to be an inherent optical property (IOP) of the ambient medium. The total absorption found in a given ocean is due to the

biological and inorganic particulates, colored dissolved organic matter (CDOM), and the absorption of pure water as expressed in equation 6. It is often the case in oceanic environments that there are fluorescent particles suspended in the water as well. The absorption coefficient of pure water in the visible spectrum is around 10^{-2}[1/m] at 450 nm and reduces to 10^{-1}[1/m] around 570 nm [7]. In general the optimal transmission window in the most oceans is near 550 nm [8].

$$a = a_p + a_{CDOM} + a_w \tag{6}$$

The Beer-Lambert law in equation 7 gives the relationship between the attenuation coefficient and transmission. Where I_o is the intensity of the propagating beam, z is the range, and a is the sum of the attenuation coefficients due to absorption and scattering of particles [8].

$$I = I_o e^{-az} \tag{7}$$

The amount of irradiance in the surrounding environment is largely responsible for the amount of background noise seen at the detector. Typically during the daytime, there are several hundred $watts/m^2$ of solar irradiance on the surface of the ocean [9]. This irradiance can vary drastically depending on the time of day and the cloud coverage. However, when LADAR is being used well below the surface of the ocean, the amount of environmental irradiance is greatly decreased. For this reason the depth of operation affects the final SNR in underwater environments. [10].

3. Implementation

3.1. Code structure

Before the range equation can be applied, three subfunctions must be developed namely the spatial and temporal distribution of the laser, the creation of a Dirac known as the target profile, and the selection of the attenuation coefficient based on a specific ocean model. The input parameter for each subfunction is given in the block diagram of figure 1.

The variable 'pulseE' is the amount of energy contained in the laser pulse. The laser pulse energy is spatially distributed by equation 3 and the beam width given by equation 4. The spatial limits of the plane that is normal to the propagation direction were defined to be three standard deviations of the Gaussian beam. The result of the spatial distribution is a 2D array that is passed to a function that temporally distributes the power according to equation 5. The second subfunction

requires a command that describes the type of scene. This is represented by the label 'wall' on the left of the block diagram. The scene generator creates a 2D array that contains the range of every sample in the observed scene. A 3D Dirac matrix is then created from the 2D scene array with a length that corresponds to the TOF limits specified by the range gate. This is commonly known as the target profile. The third subfunction specifies the oceanic model that will be used for the attenuation coefficient. It creates a vector of transmission coefficients based on the range of each array in the range gate so that the spatial distribution of transmission coefficients can be easily applied to the range equation.

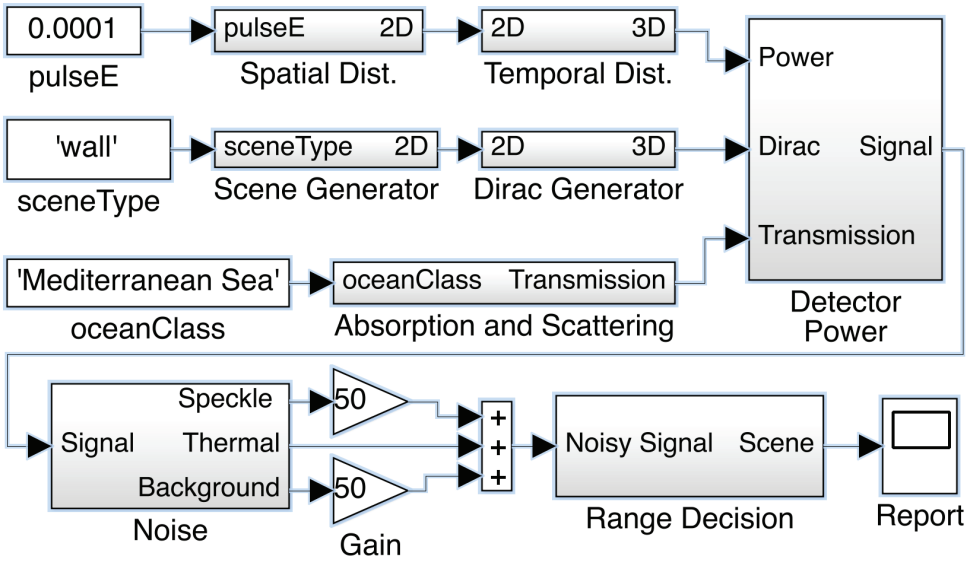

Figure 1. A block diagram showing the structure of the code.

The final distribution of energy is calculated by convolving the distributed laser power with the target profile. The resulting 3D matrix represents all of the spatial and temporal distributions in the calculation. A for-loop is then used to visit each array in the range gate to calculate the received power at the detector for each moment in time according to equation 1. Once the time varying signal of the detector array has been calculated a subfunction is called that applies speckle, thermal, and background noises to the signal. Statistical methods are used to calculate noise which is followed by applying gain. Finally the signal is passed into a decision engine for reconstructing the scene. Each sample in the photodetector array contains a time varying signal. Scene reconstruction is based on the TOF that corresponds to the maximum power for each sample in the array.

3.2. Validation

Before the oceanic model can be used for experimentation, an example scenario needs to be defined for validating the code. In this example a fiber laser module will be down converted to the optimal transmission window at 550 nm with a laser pulse energy of 0.0001[J] [11]. For the photodetector a commercially available SiAPD with an active diameter of 5 mm, a quantum efficiency of 80%, a dark current of 3 nA, a gain of 50, and a capacitance of 320 pF will be used [12].

A wall that is normal to the propagation is the simplest case because it maintains the spatial and temporal distribution of the laser pulse after it is reflected from the scene. For this reason, all validation was carried out using the wall scene. The reflectivity, the optical transmission, and the ambient transmission had a default setting of unity. Averaging techniques are assumed to completely compensate for speckle. A solar irradiance of 300 [W/m^2] will be assumed [9]. Table 1 demonstrates the accuracy of the simulation by making a comparison of the radiometric values that are expected with the results of the Matlab simulation.

Table 1. Validation of simulation with expected values.

Test Variables and Outputs		Test 1	Test 2	Test 3
Test of range 'Z'	[m]	20	1000	10000
Expected Distant Beam Width	[m]	9.00E-03	2.17E-02	2.00E-01
Matlab Distant Beam Width	[m]	9.00E-03	2.17E-02	2.00E-01
Expected Energy	[J]	6.25E-12	2.50E-15	2.50E-17
Matlab Energy	[J]	6.13E-12	2.50E-15	2.50E-17
Test of pulse energy 'pulseE'	[J]	0.001	0.0005	0.00005
Expected Energy	[J]	1.11E-10	5.56E-11	5.56E-12
Matlab Energy	[J]	1.08E-10	5.42E-11	5.42E-12
Test of transmission 'tau_atm'		0.8	0.5	0.2
Expected Energy	[J]	7.11E-12	2.78E-12	4.44E-13
Matlab Energy	[J]	6.89E-12	2.78E-12	4.17E-13
Test of reflectivity 'rho_t'		0.5	0.18	0.1
Expected Energy	[J]	5.56E-12	2.00E-12	1.11E-13
Matlab Energy	[J]	5.42E-12	1.95E-12	1.08E-13
Test of aperture 'ap_diameter'	[m]	0.008	0.004	0.001
Expected Energy	[J]	7.11E-12	1.78E-12	1.11E-13
Matlab Energy	[J]	6.93E-12	1.73E-12	1.08E-13

Table 2 validates the Gaussian distributions at 2/3 and 1/2 of the maximum values found in each distribution.

Table 2. Validation of Gaussian power distributions.

	Spatial Validation		Temporal Validation	
Gaussian Position	FWM(2/3)	FWM(1/2)	FWM(2/3)	FWM(1/2)
Expected Value	0.0162[m]	0.0212[m]	3.6021E-09[s]	4.7096E-09[s]
Matlab Result	0.0159[m]	0.0223[m]	3.6000E-09[s]	4.8000E-09[s]

4. Results

The specifications given for the laser module and the photodetector in the validation example were applied to a scene with a large wall at 20 m and a small square wall at only 10 m. A medium gray of 0.18 was used for the reflectivity of both surfaces. The input pulse energy was 1e-4 J. When this scenario was applied with no attenuation losses, the energy before gain and noise was 2.001e-12 J with total losses in the amount of -76.98dB.

The deep waters of the eastern Mediterranean Sea are estimated to have an attenuation coefficient of $0.0222[1/m]$ [13]. When the same scenario as above was used to simulate LADAR in the eastern Mediterranean Sea, the received energy before noise and gain was 1.093-12 J and the total losses amount to -79.61dB. This means that the attenuation contributed -2.616dB losses in the signal. The energy was reduced by 45% due to absorption and scattering.

A third simulation was conducted for the Mediterranean Sea with the wall distances doubled to 20 m and 40 m, the returned signal was 1.599e-13 J and the losses were -87.96dB. Doubling the distance caused an additional -8.32dB of attenuation losses which is a signal reduction of 84%. The signal reflected from the second wall was weak, so only the first wall was able to be resolved.

Figure 2 provides detailed information about the radiometric distributions at different points throughout this simulation. The effect of the spatial Gaussian distribution becomes evident in the final reconstruction of the scene in Figure 2(f). In the center of the FOV there is a larger SNR due to the laser beam intensity at the center of the pulse. The SNR ratio becomes much weaker toward the edges of the FOV such that the decision function is unable reconstruct the scene correctly. As expected, the object that is closer to the detector was able to be resolved more effectively due to a greater SNR.

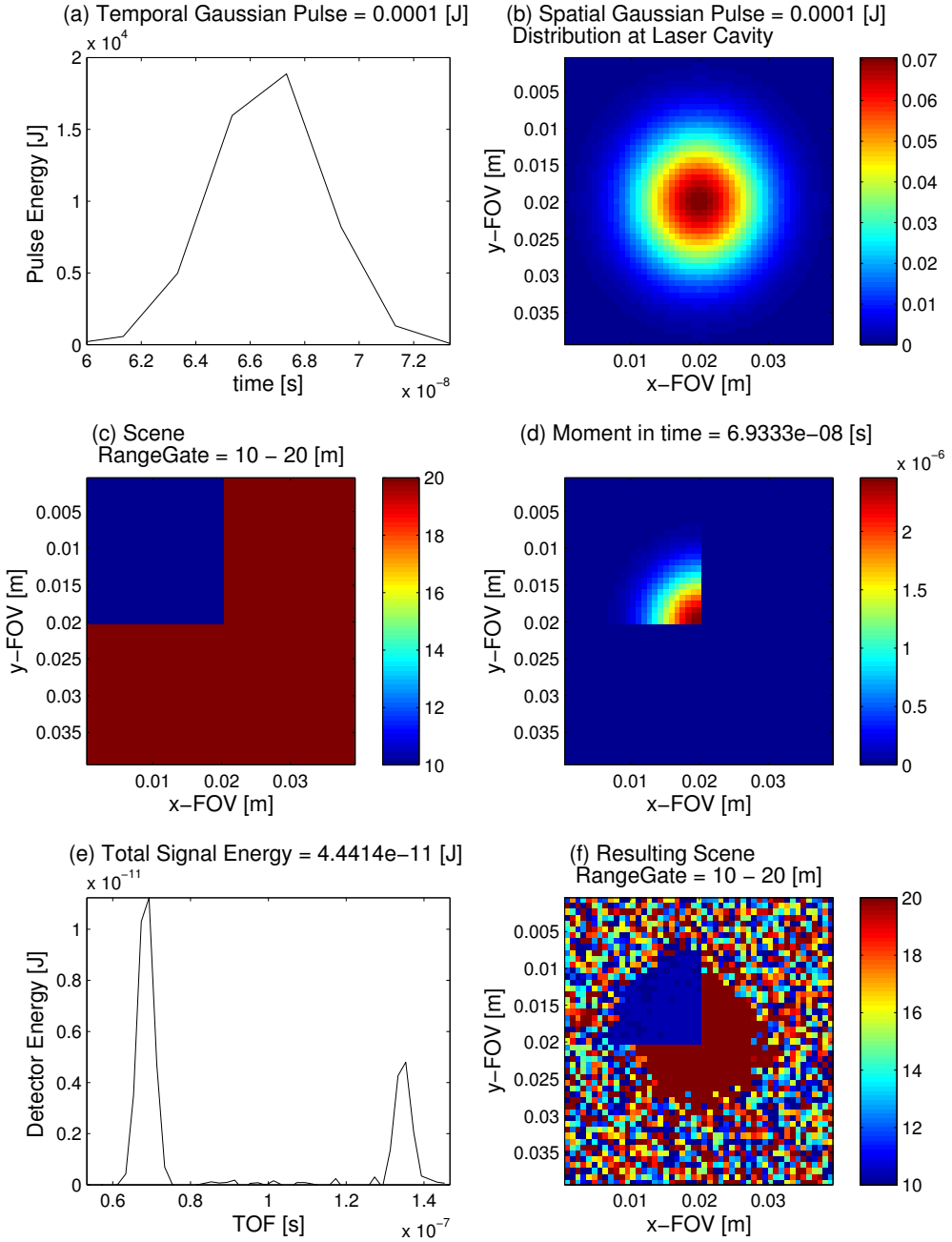

Figure 2. Radiometric results of the oceanic model (a) the temporal distribution of energy (b) the spatial distribution of energy (c) the scene is a small square at 10 meters placed in front of a much larger square at 20 meters (d) example of the photodetector signal at a specific moment (e) the photodetector energy after noise and gain versus time (f) a reconstruction of the scene.

5. Conclusions

A radiometric tool was developed in a Matlab framework for assisting in the design process of LADAR systems for use in underwater environments. The radiometric model of beam propagation in particulate media was applied and validated with various tests. The utility of the final product was demonstrated with an example LADAR system for use in the Mediterranean Sea.

Acknowledgments

The author would like to thank Prof. Santiago Royo for his help and encouragement throughout the course of this work and the Spanish Ministry of Science and Innovation, which partially supported this thesis through the Plan Nacional of I+D+i project DPI2011-25525.

References

[1] Richard D Richmond and Stephen C Cain. *Direct-detection LADAR systems*. SPIE Press, 2010.

[2] Santiago Royo Jordi Riu. A cost-effective 3d imaging lidar system. OECD CONFERENCE CENTER, 2014.

[3] Takeo Kanade, Omead Amidi, and Qifa Ke. Real-time and 3d vision for autonomous small and micro air vehicles. In *Decision and control, 2004. CDC. 43rd IEEE conference on*, volume 2, pages 1655–1662. IEEE, 2004.

[4] Michael E O'Brien and Daniel G Fouche. Simulation of 3d laser radar systems. *Lincoln Laboratory Journal*, 15(1):37–60, 2005.

[5] Seongjoon Kim, Impyeong Lee, and Yong Joon Kwon. Simulation of a geiger-mode imaging ladar system for performance assessment. *Sensors*, 13(7):8461–8489, 2013.

[6] Orazio Svelto and David C Hanna. Principles of lasers. 1998.

[7] Robin M Pope and Edward S Fry. Absorption spectrum (380–700 nm) of pure water. ii. integrating cavity measurements. *Applied optics*, 36(33):8710–8723, 1997.

[8] Weilin Hou. *Ocean Sensing and Monitoring: Optics and Other Methods*. SPIE Optical Engineering Press, 2013.

[9] Victor V. Klemas Sam J. Purkis. *Remote Sensing and Global Environmental Change*. John Wiley and Sons Ltd., 2011.

[10] Cornelius J Willers. Electro-optical system analysis and design: A radiometry perspective. Society of Photo-Optical Instrumentation Engineers (SPIE), 2013.

[11] 1.5micron compact pulsed fiber laser transmitter. www.3spgroup.com, 2014.

[12] Edmund optics avalanche photodiodes. www.edmundoptics.com, 2014.

[13] H Bradner et al. Attenuation of light in clear deep ocean water. In *Proceedings of the 2nd NESTOR International Workshop, Pylos, Greece*, page 247, 1992.